J Mater Sci: Mater Med (2011) 22:1741–1752
DOI 10.1007/s10856-011-4355-y

The effect of surface treatments on the adhesion of electrochemically deposited hydroxyapatite coating to titanium and on its interaction with cells and bacteria

Noam Eliaz · Oshrit Ritman-Hertz · Daniel Aronov · Evgeny Weinberg · Yotam Shenhar · Gil Rosenman · Miron Weinreb · Eliora Ron

Received: 13 January 2011 / Accepted: 16 May 2011 / Published online: 25 May 2011

Abstract The effect of different mechanical and chemical pre-treatments on the adhesion strength of hydroxyapatite (HAp) coating on a commercially pure titanium (CP-Ti) substrate was studied by means of a standard tensile test followed by microscopic and chemical analysis to determine the locus of fracture. In addition, the effects of either these pre-treatments or post-treatment by low-energy electron irradiation, which allowed tuning the wettability of the surface, on both osteoblast progenitor attachment and *S. aureus* bacteria attachment were investigated. A dedicated program was developed for unambiguous identification and count of stained cells. A single-phase HAp coating was formed by electrodeposition. A series of surface pre-treatments consisted of grinding down to P1000, etching in HNO_3/HF solution, grit blast, soaking in NaOH and subsequent heat treatment provided the highest adhesion strength to the HAp coating. Osteoblast progenitors derived from rats may be attached preferentially to a hydrophilic surface (post-treatment to $\theta = 30°$), while the bacteria seemed to be less attached to hydrophobic surfaces (post-treatment to $\theta = 105°$). However, the results were not statistically different. The bacteria seemed to be less attached to the smoother, uncoated surfaces.

N. Eliaz (✉) · O. Ritman-Hertz
Materials Science and Engineering Program,
Tel Aviv University, Ramat Aviv 69978, Israel
e-mail: neliaz@eng.tau.ac.il

D. Aronov · G. Rosenman
School of Electrical Engineering, Tel Aviv University,
Ramat Aviv 69978, Israel

E. Weinberg · M. Weinreb
Department of Oral Biology, Goldschleger School of Dental
Medicine, Tel Aviv University, Ramat Aviv 69978, Israel

Y. Shenhar · E. Ron
Department of Molecular Microbiology and Biotechnology,
Tel Aviv University, Ramat Aviv 69978, Israel

1 Introduction

Hydroxyapatite (HAp) coatings have been applied for approximately 30 years on orthopedic implants in order to improve their osseointegration. Plasma spraying has been the most commonly used coating technique for this purpose. However, in recent years much interest in chemical and electrochemical coating techniques has emerged. Eliaz et al. have studied different aspects of electrochemical deposition of HAp on commercially pure Ti (CP-Ti) and Ti–6Al–4V, including its nucleation and growth [1–3], the effects of bath chemistry and operating conditions [4, 5], the corrosion behavior of the coated samples [5, 6], the effect of surface pre-treatments and post-treatments on the composition, phase content, surface morphology and wettability of the coating as well as on its interaction in vitro with bone-forming cells [7], and its in vivo performance [8, 9]. In one of these studies [8], the need for improvement of the adhesion of the coating to the substrate was noted. This can be done, in principle, by either mechanical or chemical surface pre-treatments such as grit blasting [9–11], soaking in aqueous solution of NaOH and subsequent heat treatment [9, 12], or soaking in H_2O_2 [7, 13, 14]. Although the effect of such pre-treatments on the adhesion strength of electrochemically deposited HAp coating was shortly mentioned by Eliaz et al. [7], the mechanical tests were overlooked.

Another issue that has not been investigated in our previous publications is the effect of surface wettability on the attachment of bacteria. About 2% of the joint

prostheses implanted in the USA are infected, resulting in related cost, failure and disability [15, 16]. About two thirds of infections are caused by either *Staphylococcus aureus* (*S. aureus*) or *coagulase-negative staphylococci* [15, 16]. Biomaterial characteristics that affect the adsorption of bacteria to the implant surface include surface composition, topography, hydrophobicity, charge, microstructure, and rigidity. An ideal hip implant should exhibit the highest attachment of bone-forming cells and, at the same time, the minimal attachment of bacteria.

The aims of this work were: (i) to determine the effect of different pre-treatments on the adhesion strength of electrochemically deposited HAp, and (ii) to explore the effect of post-treatments on the wettability of the coating and on the attachment of both osteoblast progenitors and bacteria to it.

2 Materials and methods

2.1 Sample preparation

The substrate metal was CP-Ti Gr. 2, in the form of 5 mm thick sheet. Samples, 1×1 cm^2 in size, were cut and drilled at one face in order to provide gripping means during either pre-treatments or electrodeposition and to minimize contamination of the coated samples during handling. They were then mechanically grounded on SiC papers, from P60 to P1000 grit, washed in tap water, soaked in acetone and cleaned ultrasonically for 5 min, immersed in ethanol for 2 min, washed in Millipore deionized (Milli-DI) water, and dried in cool air. Surface activation was done by etching in a solution made of 20 vol.% nitric acid (HNO_3, 65%)—2 vol.% hydrofluoric acid (HF, 40%). The pre-treatment consisted of grinding to P1000 will be hereafter termed *Treatment #1*, while the pre-treatment consisted of grinding to P1000 followed by etching in HNO_3/HF solution will be hereafter termed *Treatment #2*.

2.2 Mechanical and chemical pre-treatments

Most samples were grit-blasted (GB) with high-purity (98.2%) white alumina powder from Calbex Mineral Trading, Inc. (Henan, China). Blasting with alumina powder was preferred over blasting with silica powder because of biocompatibility aspects [9]. The blasting machine was a model SandyPlus GD from Carlo DeGiorgi (Italy). The blasting parameters were: grit size of F200–F180 (59–68 μm), pressure of approximately 6 atm, and working distance of 3 cm or higher. The GB operation lasted until a dark grey shade evenly covered the sample. The sample was then washed in DI water and cleaned ultrasonically, as described in Sect. 2.1. The pre-treatment consisted of grinding to P1000 followed by etching in HNO_3/HF solution and then grit blast will hereafter be termed *Treatment #3*.

Some samples were soaked in a stirred solution of 5 M NaOH at 60°C for approximately 24 h. The next day, they were washed in tap water, then in running DI water, and dried in cool air. Subsequently, they were placed for 1 h in a furnace pre-heated to 600°C, and allowed to cool overnight in the furnace. The pre-treatment consisted of grinding to P1000 followed by etching in HNO_3/HF solution, grit blast and NaOH treatment will hereafter be termed *Treatment #4*. The treated samples were stored in a tightly sealed box exposed to ambient atmosphere for no longer than 3–4 days.

Some samples were alternatively soaked in a 5 M H_2O_2 solution and placed in an oven pre-heated to 60°C for 24 h. They were then washed in DI water and dried in cool air. The pre-treatment consisted of grinding to P1000 followed by etching in HNO_3/HF solution, grit blast and H_2O_2 treatment will hereafter be termed *Treatment #5*. The treated samples were stored like the NaOH-treated samples.

2.3 Electrodeposition of HAp

Electrodeposition was carried out for 2 h at 86°C, in a solution containing 0.61 mM calcium nitrate $Ca(NO_3)_2$ and 0.36 mM ammonium dihydrogen phosphate $NH_4H_2PO_4$ [5]. The pH was brought to 6.0 by addition of two drops of 1 M NaOH. After stirring, the pH was measured by an InoLab pH/Oxi Level 3 meter (WTW). The conductivity of the solution was also measured by means of a TDS/conductivity/temperature meter (CON10 series, Oakton). The electrochemical cell was placed in a water bath (Lauda Ecoline E-220T) set to 86 ± 0.1°C. The reference electrode was a saturated calomel electrode (SCE), the two counter-electrodes were made of carbon, and the working electrode was mounted on a sealed, stainless steel rod. An EG&G/PAR 263A potentionstat/galvanostat was employed to maintain the cathode potential at −1.4 V vs. SCE for 2 h. A CorrWare/CorrView (v. 2.6b) software package from Scribner Associates was used for data acquisition and data analysis.

2.4 Post-treatment

The wettability of the coated surface was tuned by an innovative process of exposure to low-energy electron irradiation, which has been described in detail elsewhere [7]. The electron irradiation system employed a commercially available electron gun (EFG-7, Kimball Physics Inc., USA). The treatment was performed in vacuum of 10^{-7}

Torr at room temperature, using electron flux with excitation energy between several tens of eV and 100 eV, and an incident charge ranging from 0 to 300 μC cm^{-2}. For osteoblast progenitor attachment tests (Sect. 2.8), the measured contact angle varied between 0° (in the as-deposited condition, i.e. without post-treatment) and 105°, in steps of 15°.

2.5 Contact angle measurements

Sessile drops of DI water at pH 5.5 were placed on the sample surface. The effect of surface heterogeneity of the studied samples was examined by measuring the contact angle hysteresis, using the tilting plate technique. The contact angle hysteresis is the difference between the advancing and the receding contact angles [17]. The optical wettability inspection was performed by a light microscope (Olympus MX-50, Opelco, USA), combining two CCD color cameras that allowed simultaneous side and top view inspection, and image analysis by means of an ImageJ 1.34s software. One of the advantages of the top view technique is that only axisymmetric drops are analyzed, leading to higher accuracy of measurements [18]. The volume of each drop was 2 μl. Ten drops were applied on each sample at different locations, to assure reproducibility and reliability of results. All measurements were carried out at 20 ± 1°C and 45 ± 5% RH (relative humidity), with an accuracy of ±1°. The contact angles were measured 10 s after the drop was deposited, which was the estimated time required to attain equilibrium with the liquid in use.

2.6 Characterization of surface chemistry, morphology and texture

X-ray photoelectron spectroscopy (XPS) measurements and analysis were performed in accordance with the procedure described elsewhere in detail [2]. The atomic ratios Ca/P and O/Ca were determined from high-resolution spectra. In order to identify unambiguously the specific CaP formed, the integrated intensity of the oxygen shake-up peaks [19] was calculated.

X-ray diffraction (XRD) was used to verify the phase content and texture. To this aim, a Θ–Θ powder diffractometer from Scintag, equipped with a liquid nitrogen-cooled germanium solid-state detector and a Cu-Kα radiation source ($\lambda = 1.5406$ Å), was used. The data was collected at a scan rate of 1°/min, from $2\Theta = 2°$ to 60°.

Environmental scanning electron microscopy (ESEM) combined with energy dispersive X-ray spectroscopy (EDS) were used to characterize the surface morphology and chemical composition as well as to determine the locus of failure that occurred during tensile adhesion tests. The ESEM (Quanta 200 FEG, FEI) enabled imaging without sputtering of a conductive layer.

2.7 Measurement of the coating/substrate adhesion strength

The strength of adhesion of the HAp coating to the metal substrate is one of the key factors determining the success or failure of the coating in vivo. Methods for measuring this property include the shear test [20–22] and the tension test [22–25]. International standards require that the value of the adhesion strength be at least 15 MPa [26].

In this work, the tension test was used. The effect of surface pre-treatments *#1* through *#5* on the coating/substrate adhesion strength was evaluated. After pre-treatment, the samples were electrodeposited with HAp, as described in Sect. 2.3.

Each test specimen was an assembly of a coated sample and a matching uncoated sample with exactly the same dimensions and surface pre-treatment. The two parts of the assembly were bonded together by a thin layer of a 3M™ Scotch-Weld™ Epoxy Adhesive DP-420 Off-White, which was left to cure at room temperature for 24 h while exposing each assembly to a compression stress of 138 kPa (20 psi). Drills were made through the largest face of the square samples in order to screw-in the matching adaptors. The adaptors, made of unquenched 1045 carbon steel, were designed to hold the sample and connect it to the grips of an MTS 20/M tensile machine. All bolts were fabricated from hardened steel. The design ensured that the coating test plane was perpendicular to the axial load. The tensile load was applied at a constant cross-head velocity of 0.5 mm min^{-1}. This velocity, which is slightly lower than that recommended in [24], was found most suitable for the samples used in this study, where both the cross-section and the thickness of the coating were smaller than the values referred to in [24]. Three assemblies were tensile tested for each surface pre-treatment. In addition to monitoring the maximum applied load, the locus of failure was determined by analyzing both parts of the assembly by means of ESEM-EDS.

2.8 Osteoblast progenitor attachment

Most samples underwent *Treatment #4* (Sect. 2.2); some of these were left uncoated (*control group #1*), while the others were coated with HAp (Sect. 2.3). *Treatment #1* (Sect. 2.1) was applied on *control group #2*, which was also left uncoated. Three samples for each contact angle were analyzed.

Osteoblast progenitors were isolated from the femora of rats (type Sprague–Dawley) that had been killed. The animal protocols were approved by the Institutional

Animal Care and Use Committee (IACUC) of the Sackler Faculty of Medicine at Tel-Aviv University. Bone marrow was extracted from the femur, and cells were cultured in flasks for 48 h in a basic medium. This medium contained the minimum essential medium eagle, alpha modification (MEM-Alpha), 13% FCS antibiotics (penicillin, streptomycin and nystatin), L-glutamine, sodium pyruvate, non-essential amino acids, and ribonuclease. The cells of interest were those that adhered to the surface of the flask; the rest were removed by rinsing with phosphate-buffered saline (PBS). This procedure was repeated 4–5 times, until no floating cells were apparent under the microscope. The adherent cells were detached using 5-ml of trypsin (0.25%)–EDTA solution (1:2000) for 7–10 min. Then, the trypsin was neutralized with an equal amount of medium (5 ml), and cells were centrifuged for 7 min at 20°C. The liquid was removed by suction, leaving only the cells at the bottom of the test tube. The desired volume (1 ml) of medium was added and vortexed. The cells were counted using a counting chamber (hemocytometer), and were further diluted to the desired concentration.

The samples were sterilized in Isopropanol. Isopropanol diluted in water (60–90 vol/o), with or without ethanol, has been widely used as a disinfectant [27, 28]. Preliminary tests showed that the sterilization process was efficient against both aerobic and anaerobic bacteria. The sterilized samples were seeded with 150 µl of the cell solution while verifying that the liquid was evenly spread. The number of cells seeded on each sample was 15,000. They were incubated for 4 days at 37°C in a 5% CO_2 humidified environment. Fixation was performed with 3% Formaldehyde for 1.5 h. Staining was established by soaking the samples in 0.01 g l^{-1} BisBenzimide Hoechst 33342 trihydrochlorate solution for 5 min. As a control, cells were also seeded on a plastic dish and stained in a crystal violet (non-fluorescent) dye for further light microscopy analysis.

The cells were imaged and counted using an Olympus IX-71 light microscope equipped with an excitation filter BP 340-380 (U-MWU2 fluorescence filter cube, wide-band UV) and an AnalySIS Docu image analysis software. Cells tend to attract one another, and often form agglomerates. Hence, it was often difficult to discriminate between different cells because their fluorescent glow overlapped. Moreover, due to the background glow, dots of stain could sometimes be mistakenly considered as cells. Another complication was the tendency of the cells to spread differently on differently treated surfaces. Consequently, different thresholds were required for different samples. In order to overcome these difficulties, a dedicated MATLAB program was written in the framework of this work. Its principle is demonstrated in Fig. 1. First, the raw image was acquired (Fig. 1a). In the second step, this image was binarized (Fig. 1b). In the third step, the features observed in Fig. 1b were colored based on the set threshold (500 pixels in this example)—Fig. 1c. In the fourth step, the number (intensity) of counted stains was calculated and presented versus the area (in pixels) of each stain (Fig. 1d). In Fig. 1d, four stains are indicated altogether, two for each of the two size bars. As the size of the scale bar in Fig. 1c is known (1600 pixels), it can be omitted from Fig. 1d. Thus, we are left with two stains of 800 pixels each, and one stain of 1600 pixels. Now, as it was established that the size of a nucleus of a single cell is $\sim$800 pixels, it can be concluded that only four cells actually reside in this field of view. It is evident that such a conclusion would not be easy to make based on Fig. 1a along, i.e. without applying the counting program.

2.9 Attachment of *S. aureus*

Four types of samples were evaluated: uncoated with *Treatment #1* (Sect. 2.1), as-deposited with HAp (*Treatment #4*, contact angle $\approx$0°), deposited with HAp (*Treatment #4*) and post-treated to 45°, deposited with HAp (*Treatment #4*) and post-treated to 105°. The fluid used for dilution in the bacteria treatment was DI water sterilized in autoclave at 120°C. Sterilized Eppendorf centrifugation tubes (Axygen) were placed in three rows, each holding nine tubes. Next, 1 ml of water was poured into each tube, which was subsequently closed. The bacteria were seeded on a plate with Lysogeny broth (Difco™ LB Broth, Lennox, BD, NJ) solidified with 2% agar. After overnight incubation, the bacteria were scratched from the plate and placed in a beaker containing 2 ml LB, and left on a shaker overnight. The bacteria reach stationary phase with a density of roughly 10^9 colony forming units (CFU) per ml. First, a test was designed to determine how long the bacteria medium should be left on the samples. Five samples were used, each one being exposed to the medium for a different time period. A time period of 3 min was found optimal, allowing to easily distinguish between colonies and to count them accurately. Next, a drop of 100 µl solution with a concentration of 10^9 CFU ml^{-1} was placed with a pipette on the sample for 3 min. The sample was moved to a different plate and washed gently with 10 ml of DI water in order to remove non-adherent bacteria. The sample was then moved to a well and washed more aggressively (10 times suction followed by dispensing) with 1 ml of water. This step was aimed to remove the adhered bacteria and enable their count. Then, 100 µl of the solution was placed in the pre-prepared Eppendorf tube and stirred (1st dilution). A second dilution was carried out, in which 100 µl of the solution in the first Eppendorf tube was diluted into the second tube and stirred. The last dilution was done similarly, into the third tube. Drops with a volume of 15 µl from each Eppendorf tube (each level of

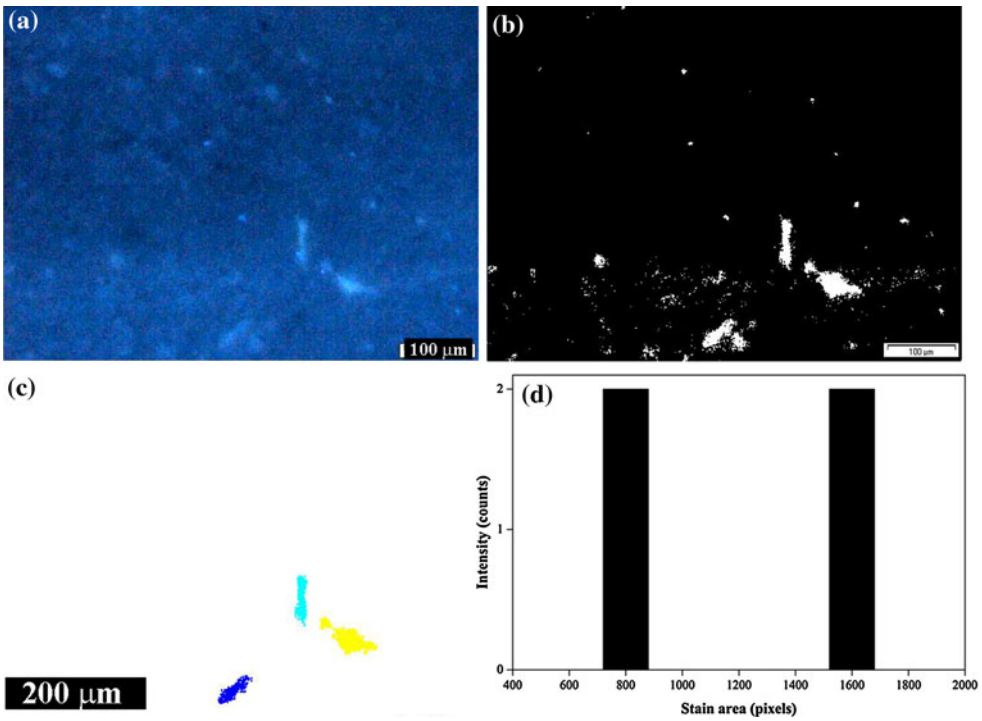

Fig. 1 The principle of operation of the MATLAB program developed in this work for counting stained cells in light microscope images. **a** The raw image is acquired, **b** The binarized form of **a**, **c** Features in **b** are *colored* based on a set threshold (500 pixels), **d** The number (intensity) of stains is drawn versus their area (in pixels). Altogether, four stains are evident, two for each of the two size *bars*. These stains include one stain related the *scale bar* in **c**, the size of which is known (1600 pixels). Thus, we are left with two "true" stains of 800 pixels each, and one stain of 1600 pixels. The size of the nucleus of a single cell is also known ($\sim$800 pixels). Thus, **d** indicates that four osteoblast progenitors are actually present in **a** (2 counts of 800 pixels and 1 count of 1600 pixels that represents two osteoblast progenitors)

dilution) were dropped on plates with LB agar. The plates were placed at 37°C in dry incubation overnight. The colonies that grew on the plates were counted after 24 h. This count relied on the assumption that the source of each colony was a single bacterium. It should be noted that due to the rough and porous surface of the electrochemically deposited HAp, some bacteria might remain attach to the surface and not be affected by washing.

2.10 Statistical analysis

The significance of the difference between different groups (pre-treatments) with respect to adhesion strength was determined by ANOVA statistical test using SPSS software. Post-hoc Tukey test was also conducted, for multiple comparisons.

When analyzing the data of osteoblast progenitor attachment, the cell distribution cannot be assumed normal. The osteoblast progenitors have a strong affinity to one another, and edge effects are apparent. This causes an uneven picture, where some fields of view have very high cell density while others are empty from cells. Hence, several approaches were examined to handle this problem without distorting the true trends. The first approach was to apply one of two data transformations—ln and square root—and to analyze the transformed data by ANOVA test. Another approach was to use the non-parametric Kruskal–Wallis test within ANOVA, which does not assume a normal distribution of the population. Multiple comparison tests were run using the Mann–Whitney test for each combination of pairs. The Bonferroni correction was applied, with $\alpha = 0.005$. Another approach was evaluated, where only the six fields of view with the highest cell density were counted for each group. The last approach was to apply the Kruskal–Wallis tests to the six fields with the highest cell density.

3 Results

3.1 The chemical composition and microstructure of the electrodeposited HAp coating

In this section, we focus on *Treatment #4* which resulted in the highest adhesion strength (Sect. 3.2) and attractive performance in vivo [9].

A survey XPS spectrum (0–1400 eV) revealed only the presence of Ca, P, O and C at the surface of the coated

sample. High-resolution XPS measurements yielded the chemical composition shown in Table 1. The C(1s) structure indicated the presence of carbonate-type carbon (binding energy ~289.3 eV), an impurity that is often incorporated in synthetic calcium phosphates due to the presence of CO_2 in the air or in solution. The presence of carbonate required adjustments like those made by Lu et al. [19]. Both the measured and adjusted Ca/P and O/Ca ratios are thus included in Table 1. The integrated intensity (i.e. peak area) of the oxygen shake-up peaks (i.e. oxygen loss spectrum) was also analyzed, following the procedure described elsewhere in detail [2]. The oxygen loss spectrum is closely related to different functional groups such as O–H and P=O. The values of the integrated intensity of $O(1s)_{II}$ normalized by the total intensity $O(1s)_{total}$ are given in Table 1, after correction related to the presence of carbonate.

A representative XRD pattern (Sample #1) is shown in Fig. 2. Phase identification was made with respect to JCPDS files 09-0432 (HAp), 21-1276 (TiO_2), 10-0173 (Al_2O_3) and 44-1294 (Ti). Among the different possible calcium phosphate phases, only HAp is evident. The measured unit cell parameters, $a = 9.423$ Å and $c = 6.878$ Å, were similar to those reported in card 09-0432 for powder HAp ($a = 9.418$ Å, $c = 6.884$ Å). The strongest HAp reflection at ~26° is (002), thus representing preferred orientation [5]. Reflections related to Ti, Al_2O_3 and TiO_2 are also evident.

ESEM images revealed that the HAp coating on NaOH pre-treated samples consisted of prismatic hexagonal bars arranged in aggregates, similar to those reported in Ref. [7], but with a smaller diameter of approximately 100 nm.

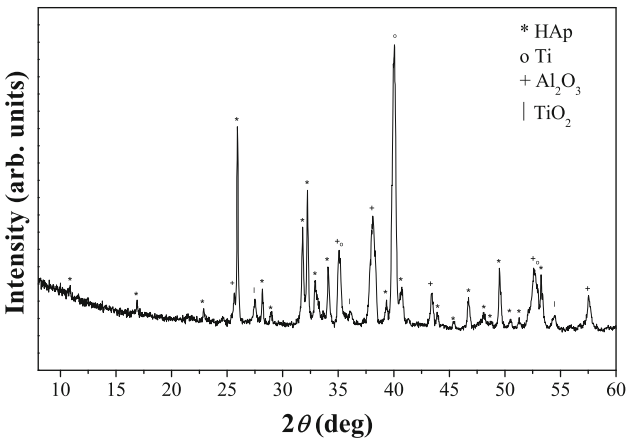

Fig. 2 XRD pattern from Sample #1. CP-Ti was pre-treated, first mechanically and then chemically with NaOH, and was subsequently electrodeposited with calcium phosphate

EDS analysis gave average Ca/P ratios of 1.72 and 1.71 in Sample #1 and Sample #2, respectively. EDS revealed also Al and Ti, in accordance with the XRD data.

3.2 The coating/substrate adhesion strength

The tensile stress to failure of each type of pre-treated samples is displayed in Fig. 3. The NaOH pre-treatment (*Treatment #4*) resulted in the highest failure stress. ANOVA test showed that the difference between the groups was statistically significant ($P = 0.041$). Post-hoc Tukey test revealed that *Treatment #1* and *Treatment #4* were statistically different ($P = 0.031$), while all other comparisons were not ($P > 0.05$).

Table 1 Chemical composition (at.%) of the CP-Ti sample pre-treated with NaOH (*Treatment #4* in Sect. 2.2) and electrodeposited with HAp, as determined by high-resolution XPS scans

	Sample #1	Sample #2	Octacalcium phosphate (OCP)	HAp
O	53.52	53.59		
Ca	17.40	17.99		
P	13.81	13.12		
C	15.27	15.30		
Ca/P, measured	1.26	1.37	Theoretical: 1.33, Ref. [19]: 1.24 ± 0.09	Theoretical: 1.67, Ref. [19]: 1.46 ± 0.09
Ca/P, adjusted	1.23	1.33		
O/Ca, measured	3.08	2.98	Theoretical: 3.625, Ref. [19]: 3.40 ± 0.20	Theoretical: 2.60, Ref. [19]: 2.74 ± 0.03
O/Ca, adjusted	3.03	2.93		
$O(1s)_{II}$/ $O(1s)_{total}$	Measured: 0.060, adjusted: 0.064	Measured: 0.066, adjusted: 0.071	Ref. [19]: 0.053 ± 0.004	Ref. [19]: 0.066 ± 0.003

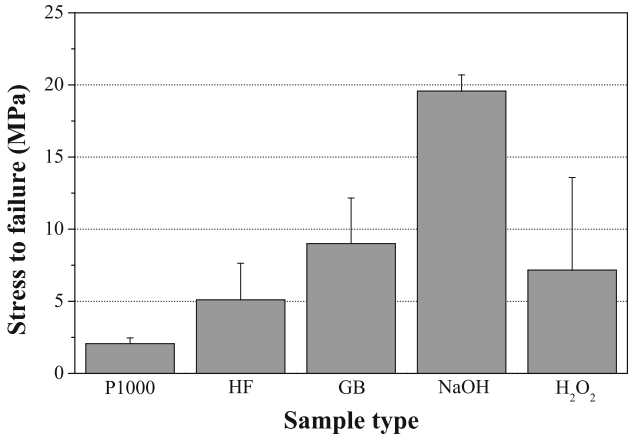

Fig. 3 The tensile stress to failure of HAp-coated samples with different pre-treatments during adhesion test. The data is presented in terms of mean + standard error of the mean ($n = 3$)

ESEM-EDS analysis was used to determine the locus of failure. Both parts of the specimen assembly were analyzed. In EDS analysis, Ca and P reflected the presence of HAp on the surface, C and Si were considered as indicators of the presence of glue at the surface, and Ti was considered as an indicator of the titanium substrate. In some of the grit-blasted samples, traces of Al were also found. In all groups, a mixed mode of failure was observed. Figure 4 shows selected ESEM images of the fractures. In the case of *Treatment #1*, one sample exhibited a region of failure between the glue and the uncoated part, while the other two samples exhibited regions of failure between the glue and the uncoated part, failure between the glue and the coated part, and failure within the glue. In the case of *Treatment #2*, all three samples exhibited regions of failure between the glue and the uncoated part, failure between the glue and the coated part, failure within the glue, and failure within the coating (cohesive failure). Two of these samples exhibited also a region of failure between the coating and the metal substrate (adhesive failure). In the case of *Treatment #3*, all three samples exhibited regions of failure within the glue and within the coating. One of these samples exhibited also a region of adhesive failure, while another sample exhibited five failure regions—including also between the glue and the coated part and between the glue and the uncoated part. In the case of *Treatment #4*, neither adhesive failure nor failure between the glue and the uncoated part was identified. Instead, all three samples failed within the glue layer, one of them also between the glue and the coated part, and another one revealed also a region of cohesive failure. In the case of *Treatment #5*, the coating started to peel-off in two of the three samples during ultrasonic cleaning prior to the gluing, thus representing poor adhesion strength and resulting in a high standard deviation in the values of stress to failure. All three samples exhibited cohesive failure, one sample showed also failure within the glue layer, another sample showed also failure within the glue layer as well as adhesive failure, and the third sample showed also adhesive failure, failure between the glue and the uncoated part and failure between the glue and the coated part.

3.3 Osteoblast progenitor attachment

The results of osteoblast progenitor attachment are summarized in Fig. 5. Figure 5a–d shows microscope images illustrating the effect of some of the treatments, whereas Fig. 5e summarizes the cell-count data. It seems that there may be some preference for osteoblast progenitor attachment on surfaces with contact angle $\theta = 30°$ or 90°, but this does not seem to be statistically significant. The groups were found significantly different after square-root transformation ($P = 0.049$), but not significantly different after ln transformation ($P = 0.120$). The Kruskal–Wallis test indicated a significant difference between groups ($P = 0.048$). The Mann–Whitney test with Bonferroni correction indicated that only two pairs were significantly different—the as-deposited HAp coating was found different from HAp post-treated to 30° ($P = 0.004$), and the HAp post-treated to 30° was found different from the HAp post-treated to 75° ($P = 0.002$). Because the fields of view for cell counting were selected blind, some fields had very high cell density while others were empty of cells. ANOVA analysis of the six fields of view per group with the highest cell density indicated significant difference among groups ($P = 0.002$); the post-hoc Tukey test showed that the groups were not significantly different. Kruskal–Wallis analysis of the six fields with the highest cell density yielded $P = 0.001$. Multiple comparisons by means of the Mann–Whitney test with the Bonferroni correction now showed significant difference between six pairs: as-deposited HAp versus HAp post-treated to 30° ($P = 0.000$), as-deposited HAp versus uncoated sample with *Treatment #1* ($P = 0.003$), as-deposited HAp versus uncoated sample with *Treatment #4* ($P = 0.001$), HAp post-treated to 15° versus HAp post-treated to 30° ($P = 0.003$), HAp post-treated to 30° versus HAp post-treated to 75° ($P = 0.001$), and HAp post-treated to 75° versus uncoated sample with *Treatment #4* ($P = 0.004$).

3.4 Attachment of *S. aureus*

Test plates after incubation are shown in Fig. 6a, demonstrating the density of the bacteria in two dilutions. The absolute number of bacteria colonies in each dilution was counted, and the results (in CFU) of at least two sets per each of four different surfaces are shown in Fig. 6b. It is apparent that the least amount of bacteria was attached to

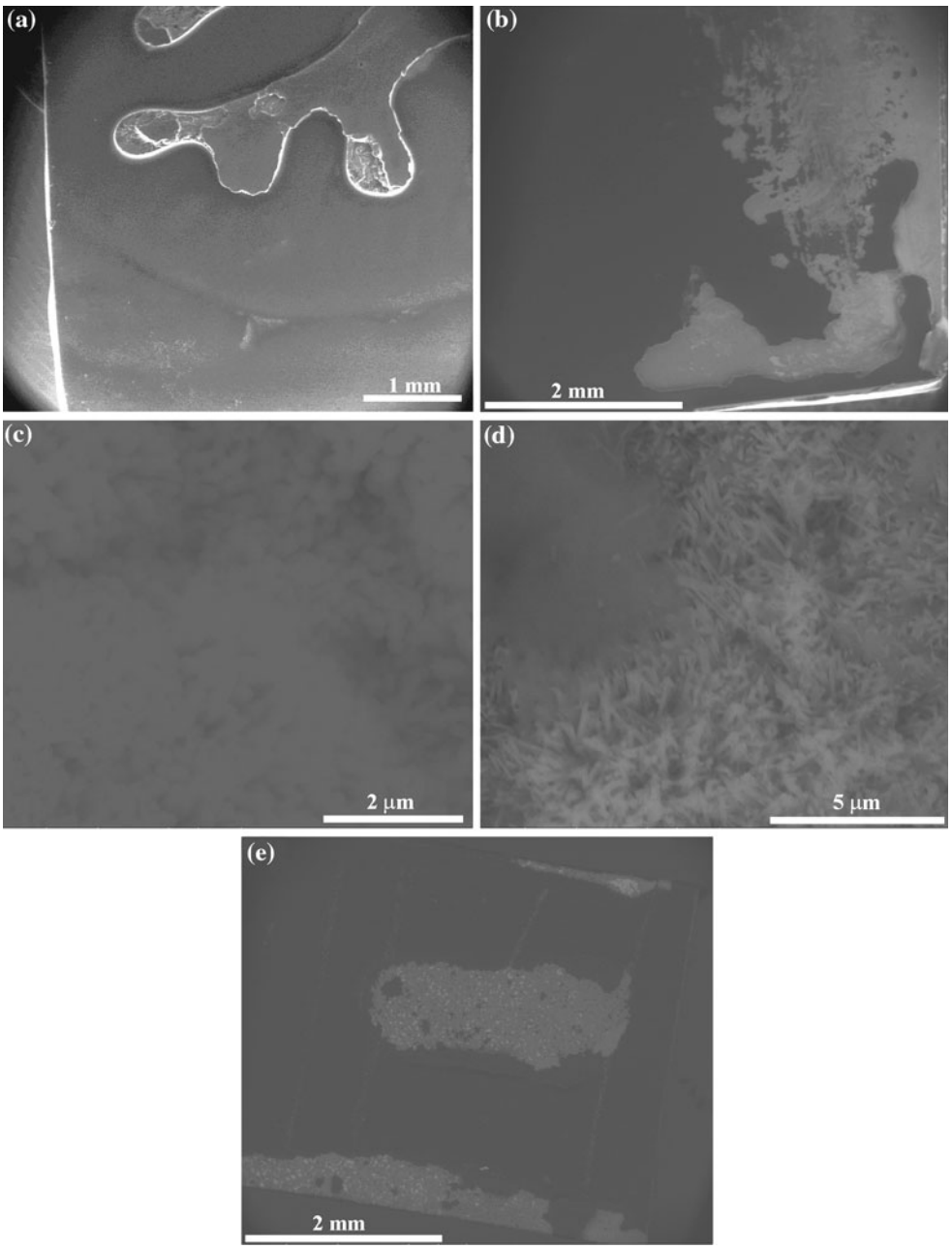

Fig. 4 ESEM images demonstrating various regions on the fracture surface of the coated part of the assembly: **a** *Treatment #1*, a sample demonstrating failure between the glue and the coated part as well as failure within the glue layer; **b** *Treatment #2*, a sample demonstrating adhesive and cohesive failure modes as well as failure within the glue layer and failure between the glue and the coated part; **c** *Treatment #3*, a sample demonstrating cohesive failure mode as well as failure within the glue layer; **d** *Treatment #4*, a sample demonstrating failure within the glue layer and failure between the glue and the coated part; **e** *Treatment #5*, a sample demonstrating adhesive and cohesive failure modes as well as failure within the glue layer

uncoated control samples with *Treatment #1*. The HAp coating post-treated to 105° (hydrophobic) seems to attach somewhat less bacteria than the as-deposited HAp, which is highly hydrophilic. Significantly higher amount of bacteria were attached to the HAp coating post-treated to 45°. One-factor ANOVA revealed statistically different group effect ($P = 0.0056$). Scheffe post-hoc test revealed significant differences only between the group post-treated to 45° and the other groups ($P < 0.05$), while all other comparisons were not statistically significant.

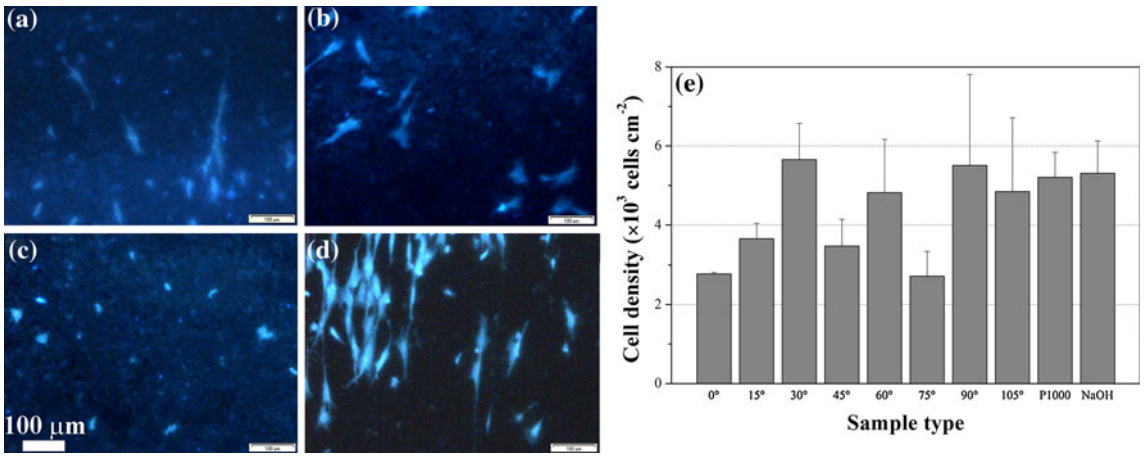

Fig. 5 Fluorescent microscope images of osteoblast progenitors derived from rats on different surfaces: **a** As-deposited HAp ($\theta \sim 0°$), **b** HAp post-treated to $\theta = 45°$, **c** HAp post-treated to $\theta = 75°$, and **d** uncoated control sample (*Treatment #1*). All coated samples underwent *Treatment #4*. The cell counts are presented in **e** in terms of mean + standard error of the mean ($n = 3$)

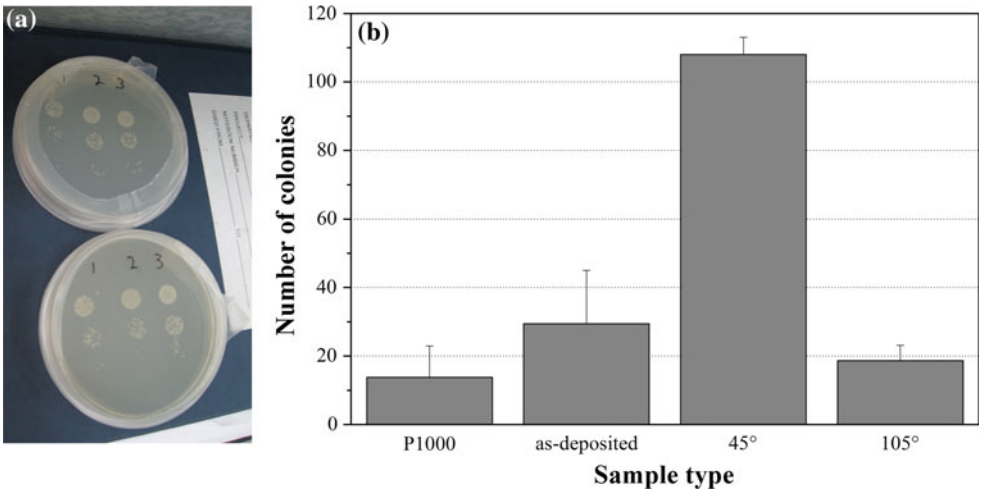

Fig. 6 **a** Bacterial attachment test plates. Each *dot* in each *circle* represents a colony, which is assumed to have originated from a single bacterium. **b** Bacteria counts (CFU) on four different surfaces (mean + standard error of the mean). All coated samples underwent *Treatment #4*

4 Discussion

4.1 The phase content of the electrodeposited HAp coating

The chemical composition and phase content of the coating were determined by high-resolution XPS combined with advanced analysis of the oxygen shake-up (satellite) peaks. Both the as-measured and the adjusted values of Ca/P, O/Ca and $O(1s)_{II}/O(1s)_{total}$ are listed in Table 1 and compared to the theoretical values as well as to the values reported by Lu et al. [19]. The two phases of interest are HAp and OCP; the latter has been found to be a precursor phase in our previous publications [2, 9]. Based on Table 1, the coating may consist of HAp, OCP and/or tricalcium phosphate (TCP). However, XRD revealed only HAp, with a preferred (002) orientation (see Fig. 2). EDS analysis also gave Ca/P ratios that meet the FDA requirement for a Ca/P ratio of at least 1.67 in HAp coatings [28].

XRD revealed also Ti, TiO_2 and Al_2O_3 phases (Fig. 2). The presence of Ti and Al was also found by EDS. The appearance of Ti indicates that the coating is either thin or porous. The strongest reflection of Ti in Fig. 2 is at $\sim 40°$, and represents a (101) orientation. Hence, no heteroepitaxial growth of HAp can be claimed, in contrast to our previous publications [1, 5, 7]. This difference may be attributed to the different pre-treatments, in particularly the use of grit blast in the present work. The TiO_2 reflections may represent either the native oxide on Ti or the product of surface pre-treatment. The alumina reflections are probably related to residues of alumina powder used in the grit blast process.

4.2 The effect of surface pre-treatments on the strength of adhesion of electrochemically deposited HAp to titanium

Figure 3 shows the effect of different mechanical and chemical surface pre-treatments on the strength of adhesion

under tension of the HAp coating to the CP-Ti substrate. It demonstrates how a series of pre-treatments gradually increased the adhesion strength, from *Treatment #1* where only grinding to P1000 was applied, to *Treatment #4* where grinding to P1000 was followed by etching in HNO_3/HF solution, grit blast, soaking in NaOH and subsequent heat treatment. *Treatment #4* is the only pre-treatment that provides sufficiently high adhesion strength to satisfy the requirements of international standards (see Sect. 2.7). The microscopic evaluation of the locus of failure (Fig. 4) showed that following *Treatment #4*, no separation occurred at the interface between the coating and the metal substrate even at the failure stress. This trend is supported by unpublished data by Eliaz and Kopelovitch, where the adhesion strength of the coating was measured under shear stress after different surface pre-treatments. In that study, the average stress to failure was the lowest for P1000 ground CP-Ti (7.3 MPa), higher for P1000 and HF/HNO_3 pretreated samples (13.7 MPa), and even higher for P1000, HF/HNO_3 and grit-blasted samples (20.7 MPa). When soaking in NaOH was added on top of the last treatment, the acrylic holder failed.

It has been reported that two types of factors may affect the results of the adhesion test. The first type is the intrinsic quality of the coating, which is expressed in terms of the energy required to break chemical bonds. The second type is extrinsic, e.g. mechanical components [29]. The relative smoothness of the sample ground to P1000 may be responsible for the glue not attaching strongly to the uncoated part of the specimen assembly. In contrast, both chemical etching in HF/HNO_3 and grit blast led to a rougher surface, thereby increasing the surface area on which the coating is formed. In the case of the NaOH pre-treatment, the glue failed before the coating. Hence, the actual adhesion strength of the HAp coating is even higher than the value shown in Fig. 3. There seems to be a correlation between the surface roughness and the stress to failure—as the former is increased, the latter increases to. This finding is supported by the work of de Senna et al. [30], who evaluated the effect of different surface finishes on the adhesion of electrophoretically deposited HAp on Ti. The NaOH pre-treatment provides higher adhesion strength than the H_2O_2 pre-treatment. The former treatment has been found to significantly increase the bond strength of bone to uncoated titanium rods in rabbit femora [31]. An in vivo study [9] has recently demonstrated enhanced osseointegration of electrochemically deposited HAp on Ti–6Al–4V alloy due to a pre-treatment consisted of soaking in NaOH without subsequent heat treatment. In addition, that coating exhibited reduced occurrence of delamination compared to the commercial plasma-sprayed HAp coating. Taking into account also the higher osteoblastic cell density that has been measured on HAp following NaOH pre-treatment [7], this treatment seems most attractive for orthopedic and dental implants.

4.3 The attachment of bone-forming cells

The effect of different surface pre- and post-treatments on the attachment of osteoblast progenitors was demonstrated in Sect. 3.3. A dedicated MATLAB program was developed for counting stained cells in the fluorescent microscope images (Sect. 2.8). The surface energy of implants significantly influences tissue response. Baier et al. studied the effect of surface energy on the biological response to tantalum [32], germanium and Co–Cr–Mo [33] implants. High surface energy (hydrophilic) implants were associated with an enhanced fibroblast cell response. Aronov et al. [34] have tuned the wettability of HAp ($10° < \theta < 100°$) by means of the same post-treatment used in the present work and found that DNA tended to bind to surfaces with $\theta < 50°$. In contrast, bovine serum albumin (BSA) protein, which contains hydrophobic domains, bound preferentially to surfaces with $\theta > 50°$. The surface energy has also been shown to affect the bone cell maturation and differentiation [35] and the osseointegration [36]. Eriksson et al. [37] found that the cellular reaction was different for hydrophilic and hydrophobic implants, especially in the initial stages of wound healing. Surfaces with a higher surface energy showed more rapid cell activation and differentiation than those with lower surface energy.

In the present study, osteoblast progenitors seemed to attach preferentially to HAp post-treated to $\theta = 30°$ or 90°, although this tendency was not statistically significant. A preferential attachment to HAp surface post-treated to 30° was observed when MBA-15 osteogenic cell line was used instead of osteoblast progenitors derived from rats (unpublished data). The adhesion and proliferation of osteoblasts have been correlated with substratum wettability, the cells exhibiting a strong preference for hydrophilic substrata [38]. Such a preference has recently been supported by Eliaz et al. [7]. It should be borne in mind, however, that when relating the relative biological interaction with surface energy, there may be an optimal biocompatibility zone with respect to the critical surface tension (or surface free energy) [39]. Thus, the present study should be extended, analyzing a significantly higher number of samples per contact angle. It should be noted that the conversion of contact angles to surface energies is not straightforward in the case of porous surfaces, like the HAp coatings studied in this work. In this case, models such as those proposed by Wenzel and by Cassie and Baxter must be considered [40–42].

4.4 The attachment of *S. aureus*

The results presented in Fig. 6 and in Sect. 3.4 indicate that less bacteria were attached to the uncoated samples as compared to the HAp-coated samples, and that among the coated samples—those post-treated to $\theta = 105°$ attached less bacteria than those without post-treatment, and significantly less bacteria than those post-treated to $\theta = 45°$. Vogely et al. [43] performed an in vivo study and found that more *S. aureus* bacteria attached to HAp-coated Ti–6Al–4V implants than to uncoated implants following four-week implantation, no matter the level of contamination prior to implantation was. Rosenman and Aronov [44] applied on HAp the same post-treatment as that used in the present study and investigated the adhesion of three types of bacteria: *Escherichia coli*, *Pseudomonas putida*, and *Bacillus subtilis*. It was found that while *Escherichia coli* adhered to surfaces with $\theta = 30°$, it made an intermediate reaction with surfaces with either $\theta = 20°$ or $\theta = 40°$, and no reaction with surfaces with $\theta = 60°$, 80° or 100°. In contrast, *Pseudomonas putida* adhered to surfaces with $\theta = 80°$ and made an intermediate reaction with surfaces with $\theta = 100°$, and no reaction with surfaces with $\theta = 20°$, 30°, 40°, or 60°. *Bacillus subtilis* adhered to surfaces with $\theta = 100°$ and made an intermediate reaction with surfaces with $\theta = 80°$, and no reaction with surfaces with $\theta = 20°$, 30°, 40°, or 60°. Thus, it seems that the low-energy electron irradiation post-treatment has the potential of tailoring HAp-coated surfaces to resist infection by specific types of bacteria.

In the present study it was found difficult to detach the bacteria from the pores of the HAp coating. Based on our results, it might not be possible to tailor a HAp surface with maximal osteoblast cell attachment and minimal *S. aureus* bacteria attachment, just by tuning the contact angle (surface energy), because while the first condition may require a hydrophilic surface, the second condition seems to require a hydrophobic surface. However, this conclusion should be verified further by monitoring the effect of additional contact angles and increasing the number of samples per contact angle. For example, based on Fig. 5, post-treatment to $\theta = 90°$ may eventually be found as a reasonable compromise between the two conditions.

5 Conclusions

In this research, the effect of different mechanical and chemical pre-treatments on the strength of adhesion under tension of electrochemically deposited HAp coating to CP-Ti substrate was studied. In addition, the effects of either pre-treatments or a post-treatment by low-energy electron irradiation, which changes the wettability of the surface, on both osteoblast progenitor attachment and *S. aureus* bacteria attachment were investigated. The following conclusions were drawn:

(1) A series of surface treatments, consisted of grinding down to P1000, etching in HNO_3/HF solution, grit blast, soaking in NaOH and subsequent heat treatment, provided the highest adhesion strength to the HAp coating. The stress to failure increased as the surface roughness of the substrate was increased by pre-treatments. The NaOH treatment was found to be better than the H_2O_2 treatment and seems most attractive for orthopedic and dental applications.

(2) Osteoblast progenitors may be attached preferentially to HAp post-treated to $\theta = 30°$ (hydrophilic surface), although this tendency was not statistically significant, e.g. in comparison to post-treatment to $\theta = 90°$. On the other hand, *S. aureus* bacteria seemed to be less attached to hydrophobic surfaces (HAp post-treated to $\theta = 105°$). Thus, it might not be possible to tailor a HAp surface with maximal osteoblast cell attachment and minimal *S. aureus* bacteria attachment, at the same time, just by tuning the surface energy. Less bacteria were attached to the smoother, uncoated surfaces.

Acknowledgments We thank Mario Levinshtein and William Kopelevich from the Biomaterials and Corrosion Laboratory for their technical assistance and fruitful discussions, respectively. We also thank Dr. Larisa Burstein and Dr. Yuri Rosenberg from the Wolfson Applied Materials Research Centre for their XPS and XRD characterization service, respectively.

References

1. Eliaz N, Eliyahu M. Electrochemical processes of nucleation and growth of hydroxyapatite on titanium supported by real-time electrochemical atomic force microscopy. J Biomed Mater Res A. 2007;80:621–34.
2. Eliaz N, Kopelovitch W, Burstein L, Kobayashi E, Hanawa T. Electrochemical processes of nucleation and growth of calcium phosphate on titanium supported by real-time quartz crystal microbalance measurements and X-ray photoelectron spectroscopy analysis. J Biomed Mater Res A. 2009;89:270–80.
3. Eliaz N. Electrocrystallization of calcium phosphates. Isr J Chem. 2008;48:159–68.
4. Sridhar TM, Eliaz N, Mudali UK, Raj Baldev. Electrophoretic deposition of hydroxyapatite coatings and corrosion aspects of metallic implants. Corros Rev. 2002;20:255–93.
5. Eliaz N, Sridhar TM. Electrocrystallization of hydroxyapatite and its pH dependence. Cryst Growth Des. 2008;8:3965–77.
6. Eliaz N, Sridhar TM, Mudali UK, Raj Baldev. Electrochemical and electrophoretic deposition of hydroxyapatite for orthopaedic applications. Surf Eng. 2005;21:238–42.
7. Eliaz N, Shmueli S, Shur I, Benayahu D, Aronov D, Rosenman G. The effect of surface treatment on the surface texture and contact angle of electrochemically deposited hydroxyapatite

coating and on its interaction with bone-forming cells. Acta Biomater. 2009;5:3178–91.
8. Wang H, Eliaz N, Xiang Z, Hsu HP, Spector M, Hobbs LW. Early bone apposition in vivo on plasma-sprayed and electrochemically deposited hydroxyapatite coatings on titanium alloy. Biomaterials. 2006;27:4192–203.
9. Lakstein D, Kopelovitch W, Barkay Z, Bahaa M, Hendel D, Eliaz N. Enhanced osseointegration of grit-blasted, NaOH-treated and electrochemically hydroxyapatite-coated Ti–6Al–4V implants in rabbits. Acta Biomater. 2009;5:2258–69.
10. Feighan JE, Goldberg VM, Davy D, Parr JA, Stevenson S. The influence of surface-blasting on the incorporation of titanium-alloy implants in a rabbit intramedullary model. J Bone Joint Surg Am. 1995;77:1380–95.
11. Reikeras O, Gunderson RB. Excellent results of HA coating on a gritblasted stem: 245 patients followed for 8–12 years. Acta Orthop Scand. 2003;74:140–5.
12. Xue W, Liu X, Zheng XB, Ding C. In vivo evaluation of plasma sprayed titanium coating after alkali modification. Biomaterials. 2005;26:3029–37.
13. Park JH, Lee YK, Kim KM, Kim KN. Bioactive calcium phosphate coating prepared on H_2O_2-treated titanium substrate by electrodeposition. Surf Coat Technol. 2005;195:252–7.
14. Rohanizadeh R, Al-Sadeq M, LeGeros RZ. Preparation of different forms of titanium oxide on titanium surface: effects on apatite deposition. J Biomed Mater Res A. 2004;71:343–52.
15. Darouiche RO. Treatment of infections associated with surgical implants. New Engl J Med. 2004;350:1422–9.
16. Hudson MC, Ramp WK, Frankenburg KP. *Staphylococcus aureus* adhesion to bone matrix and bone-associated biomaterials. FEMS Microbiol Lett. 1999;173:279–84.
17. Kwok DY, Neumann AW. Contact angle measurement and contact angle interpretation. Adv Colloid Interface Sci. 1999;81:167–249.
18. del Rio OI, Neumann AW. Axisymmetric drop shape analysis: computational methods for the measurement of interfacial properties from the shape and dimensions of pendant and sessile drops. J Colloid Interface Sci. 1997;196:136–47.
19. Lu HB, Campbell CT, Graham DJ, Ratner BD. Surface characterization of hydroxyapatite and related calcium phosphates by XPS and TOF-SIMS. Anal Chem. 2000;72:2886–94.
20. ASTM F 1044-05: Standard test method for shear testing of calcium phosphate coatings and metallic coatings. ASTM International, West Conshohocken, PA.
21. Wei M, Ruys AJ, Milthorpe BK, Sorrell CC, Evans JH. Electrophoretic deposition of hydroxyapatite coatings on metal substrates: a nanoparticulate dual-coating approach. J Sol-Gel Sci Tech. 2001;21:39–48.
22. Briggs EP, Walpole AR, Wilshaw PR, Karlsson M, Pålsgård E. Formation of highly adherent nano-porous alumina on Ti-based substrates: a novel bone implant coating. J Mater Sci Mater Med. 2004;15:1021–9.
23. ASTM F 1147-05: Standard test method for tension testing of calcium phosphate and metallic coatings. ASTM International, West Conshohocken, PA.
24. ASTM C 633-01: Standard test method for adhesion or cohesion strength of thermal spray coatings. ASTM International, West Conshohocken, PA.
25. BS ISO 13779-4:2002: Implants for surgery—Hydroxyapatite—Part 4: determination of coating adhesion strength. British Standards Institution, London, UK.
26. BS ISO 13779-2:2000: Implants for surgery—Hydroxyapatite—Part 2: coatings of hydroxyapatite. British Standards Institution, London, UK.
27. Ali Y, Dolan MJ, Fendler EJ, Larson EL. Alcohols. In: Block SS, editor. Disinfection, sterilization and preservation. Philadelphia, PA: Lippincott Williams & Wilkins; 2001. p. 229–54.
28. Callahan TJ, Gantenberg JB, Sands BE. Calcium phosphate (Ca-P) coating draft guidance for preparation of Food and Drug Administration (FDA) submissions for orthopedic and dental endosseous implants. In: Horowitz E, Parr JE, editors. ASTM STP 1196: characterization and performance of calcium phosphate coatings for implants. PA: ASTM; 1994, p. 185–197.
29. Mittal KL, editor. Adhesion measurement of films and coatings. Utrecht: VSP; 1995.
30. de Sena LA, de Andrade MC, Rossi AM, de Almeida Soares G. Hydroxyapatite deposition by electrophoresis on titanium sheets with different surface finishing. J Biomed Mater Res. 2002;60:1–7.
31. Nishiguchi S, Fujibayashi S, Kim HM, Kokubo T, Takashi Nakamura T. Biology of alkali- and heat-treated titanium implants. J Biomed Mater Res A. 2003;67:26–35.
32. Meenaghan MA, Natiella JR, Moresi JL, Flynn HE, Wirth JE, Baier RE. Tissue response to surface-treated tantalum implants: preliminary observations in primates. J Biomed Mater Res. 1979;13:631–43.
33. Baier RE, Meyer AE, Natiella JR, Natiella RR, Carter JM. Surface properties determine bioadhesive outcomes: methods and results. J Biomed Mater Res. 1984;18:337–55.
34. Aronov D, Rosen R, Ron EZ, Rosenman G. Tunable hydroxyapatite wettability: effect on adhesion of biological molecules. Proc Biochem. 2006;41:2367–72.
35. Zhao G, Schwartz Z, Wieland M, Rupp F, Geis-Gerstorfer J, Cochran DL, Boyan BD. High surface energy enhances cell response to titanium substrate microstructure. J Biomed Mater Res A. 2005;74:49–58.
36. Kilpadi DV, Lemons LE. Surface energy characterization of unalloyed titanium implants. J Biomed Mater Res. 1994;28:1419–25.
37. Eriksson C, Nygren H, Ohlson K. Implantation of hydrophilic and hydrophobic titanium discs in rat tibia: cellular reactions on the surfaces during the first 3 weeks in bone. Biomaterials. 2004;25:4759–66.
38. Lim JY, Liu XM, Vogler EA, Donahue HJ. Systematic variation in osteoblast adhesion and phenotype with substratum surface characteristics. J Biomed Mater Res A. 2004;68:504–12.
39. Baier RE. Applied chemistry at protein interfaces. Adv Chem Ser. 1975;145:1–25.
40. Bormashenko E, Pogreb R, Whyman G, Bormashenko Y, Erlich M. Vibration-induced Cassie-Wenzel wetting transition on rough surfaces. Appl Phys Lett. 2007;90:201917.
41. Lafuma A, Quere D. Superhydrophobic states. Nat Mater. 2003;2:457–60.
42. Wenzel RN. Resistance of solid surfaces to wetting by water. Industr Eng Chem. 1936;28:988–94.
43. Vogely HC, Oosterbos CJM, Puts EWA, Nijhof MW, Nikkels PGJ, Fleer A, Tonino AJ, Dhert WJA, Verbout AJ. Effects of hydroxyapatite coating on Ti–6Al–4V implant-site infection in a rabbit tibial model. J Orthop Res. 2000;18:485–93.
44. Rosenman G, Aronov D. Wettability engineering and bioactivation of hydroxyapatite nanoceramics. In: Proc Intern Tech Proc Nanotech Conf, Boston, MA: 2006;2:91–4.